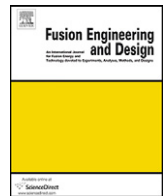




Contents lists available at [SciVerse ScienceDirect](http://SciVerse.ScienceDirect)

Fusion Engineering and Design

journal homepage: www.elsevier.com/locate/fusengdes



Modification of the electron energy distribution function during lithium experiments on the National Spherical Torus Experiment

M.A. Jaworski^{a,*}, M.G. Bell^a, T.K. Gray^b, R. Kaita^a, J. Kallman^a, H.W. Kugel^a, B. LeBlanc^a, A.G. McLean^b, S.A. Sabbagh^c, V.A. Soukhanovskii^d, D.P. Stotler^a, V. Surla^e

^a Princeton Plasma Physics Laboratory, United States

^b Oak Ridge National Laboratory, United States

^c Columbia University, United States

^d Lawrence Livermore National Laboratory, United States

^e University of Illinois at Urbana-Champaign, United States

ARTICLE INFO

Article history:
Available online xxx

Keywords:
Langmuir probe
Lithium plasma-facing component
Electron distribution function

ABSTRACT

The National Spherical Torus Experiment (NSTX) has recently studied the use of a liquid lithium divertor (LLD). Divertor Langmuir probes have also been installed for making measurements of the local plasma conditions. A non-local probe interpretation method is used to supplement the classical probe interpretation and obtain measurements of the electron energy distribution function (EEDF) which show the occurrence of a hot-electron component. Analysis is made of two discharges within a sequence that exhibited changes in plasma fueling efficiency. It is found that the local electron temperature increases and that this increase is most strongly correlated with the energy contained within the hot-electron population. Preliminary interpretative modeling indicates that kinetic effects are likely in the NSTX scrape-off layer (SOL) plasma. The decrease in plasma fueling efficiency, increase in local temperature, and increase in hot-electron fraction are all consistent with an absorbing surface intercepting the SOL plasma.

© 2011 Elsevier B.V. All rights reserved.

1. Introduction

Plasma wall conditioning and the plasma-material interactions have presented a significant challenge to fusion research for some time. Energy confinement time, stability and other metrics often improve with the application of various wall conditioning procedures. Boron is often employed for this purpose, but recent experiments have led to more wide-spread use of lithium as a wall-conditioning material. TFTR showed improvements in plasma performance by lithium conditioning of its graphite limiter [1]. CDX-U demonstrated energy confinement time increases with greater lithium coverage of its limiting surfaces in the form of both liquid and solid coatings [2]. FTU demonstrated improvements in performance with the usage of a liquid lithium limiter [3]. Many other experiments are also exploring this material in experiments detailed further in these proceedings. NSTX has also demonstrated plasma performance improvements with the application of evaporated lithium to its divertor and other plasma facing surfaces [4]. These studies all demonstrate modifications of the bulk plasma, but do not address the issue of how the wall conditioning is modifying

the local plasma that is in direct contact with the plasma facing component (PFC).

The liquid lithium divertor (LLD) was installed and tested in NSTX in order to provide an initial assessment of a porous molybdenum plasma-facing component with evaporated lithium coatings and the associated plasma-material interactions (PMI) [5,6]. In addition to the extensive core diagnostics available on NSTX, new divertor diagnostics were installed alongside the LLD [7,8]. This work focuses on the Langmuir probes used to diagnose the near-surface plasma.

Langmuir probes provide a direct measure of the net current collected by a biased electrode in a plasma [9]. Although simple in implementation, relating the electron and ion currents to plasma fluid observables has remained an issue of debate. It is possible to formulate a theory describing the electron current channel based on transport arguments [10] although such theories have been criticized [9] due to reliance on anomalous cross-field transport terms. At present, the consensus is that the region of an I - V characteristic below floating potential can be utilized for the determination of a plasma electron temperature [11]. This is referred to as the "classical" interpretation [12]. In general, this reveals a mere 5% of the electron distribution – the high energy tail. Without the ability to view the bulk of the plasma electrons, non-Maxwellian effects are not diagnosable with the

* Princeton Plasma Physics Laboratory, United States. Tel.: +1 609 243 2711.
E-mail address: mjaworsk@pppl.gov (M.A. Jaworski).

classical interpretation potentially leading to erroneous measurements [13].

Indications of such effects are evident in experiment and kinetic simulations. Experimentally, comparisons have been made between divertor Langmuir probes and divertor Thomson scattering on ASDEX [14] and DIII-D [15]. On DIII-D, it was found that the Langmuir probes yielded consistently higher electron temperatures which would be expected if the classical interpretation were used in the presence of a high-temperature tail population [13]. In ASDEX, the probe-based electron temperature was found to be a factor of two greater than the laser scattering during quiescent plasma conditions. Additionally, the Thomson scattering on ASDEX gave some indications of non-Maxwellian characteristics. In simulations of charged particles in the SOL, non-Maxwellian EEDFs are a common feature. Independent simulations by Chodura [16] and Batishchev et al. [17] both show that sharp spatial gradients arising from a recycling boundary were found to give rise to non-Maxwellian distributions at a divertor target plate. In addition to gradient effects, electron interactions with neutrals and ions can lead to non-Maxwellian distributions [18].

This paper presents Langmuir probe measurements obtained during the recent LLD experiments on NSTX. The classical and non-local approaches to probe interpretation are both utilized and compared. This is the first time the non-local approach has been applied to Langmuir probes in the divertor of a toroidal device. The impact of the evolving surface of the LLD on the SOL plasma is measured with the use of these probes and a heuristic model is proposed to account for the observations in light of the kinetic treatments of the SOL. Finally, preliminary interpretative model simulations are shown which assess the degree of collisionality of the SOL and the likelihood of the hypothesis.

2. Theory

Standard practice in the interpretation of tokamak Langmuir probes has been to assume the existence of a single Boltzmann fluid [9–11] and fit the data to the following equation:

$$I_{pr} = I_{sat}^+ \left[1 - \exp\left(-\frac{V_{pr} - V_{fl}}{T_e}\right) \right] \quad (1)$$

where I_{pr} is the probe current, I_{sat}^+ is the ion saturation current, V_{pr} and V_{fl} are the probe and floating potentials, respectively, and T_e is the electron temperature. One will notice, however, that Eq. (1) already has inaccuracies in that even though the electrons form the fluid under question, it is the *ion current* that is used in the fit, as opposed to the electron current as is the case with non-magnetized discharge probe interpretation [19,20].

One can determine if depletion of the plasma in the flux-tube attached to the probe is operating by considering the balance of fluxes into and out of that flux-tube. Define the fraction ϕ as follows:

$$\phi \equiv \frac{\Gamma_{\perp} A_{\perp}}{\Gamma_{\parallel} A_{\parallel}} \approx \frac{D_{\perp} L}{\bar{c}_e D_h^2} \quad (2)$$

where the flux, Γ is given in both perpendicular (\perp) and parallel (\parallel) directions across the respective areas, A . At the limit of electron saturation, the plasma supplies, in the parallel direction, the mean thermal velocity, \bar{c}_e . The length terms, L and $D_h = 2ab/(a+b)$ are the length of the flux tube and the “hydraulic” diameter (a term borrowed from hydrodynamics), respectively. The collection point is defined as having a rectangular cross section with side lengths of a and b . When the value of ϕ is much greater than one, then cross-field transport can supply more particles than are removed by the free-streaming parallel particle flux. In the case where ionizations are occurring inside the flux-tube, then an additional particle source is added to the numerator, relaxing the conditions on ϕ .

Table 1

Scale length estimation for the NSTX divertor plasma.

Method	n_e, m^{-3}	T_e, eV	λ_e, m	λ_{pr}, m
Classical	1 (10^{20})	15	0.023	6 (10^{-4})
Non-local	1.4 (10^{20})	8	0.005	6 (10^{-4})

For Bohm-like diffusion [21] ϕ can be further simplified to the following:

$$\phi \approx 0.06 \frac{L}{BD_h^2} \sqrt{\frac{\pi m_e T_e}{8e}} \quad (3)$$

where B is the magnetic field strength in T , T_e is given in eV and the other terms are in SI units. This is a conservative approximation as the cross-field transport is often found to be in excess of Bohm transport [21,22]. In the case of the NSTX SOL, a typical connection length is 20 m, mean temperatures based on target data and upstream MPTS measurements are about 20 eV along a flux-tube and $B \approx 0.5 T$. The probes under consideration in this study are 2 mm \times 7 mm in surface area but due to the field-line angle-of-attack, the projected dimensions are about 2 mm \times 0.6 mm. For a probe of this size then we find $\phi \approx 20$. Considering the conservative nature of this estimate for the reasons above, one would not expect the flux-tube to suffer depletion effects.

In order to address the I - V characteristic in the region beyond the floating potential, a more comprehensive probe theory is sought. In certain circumstances, it can be shown that the non-local approach is usable [12,23–25]. Although the method is developed in these references, it is repeated here due to its relative novelty. The essence of this approach is that the energy scale length of the electrons, λ_e , in the plasma is much larger than the spatial scale of the probe such that [24,26]:

$$\lambda_e = \left[\frac{4D_e}{\nu_e + \delta\nu_a + \nu^*} \right]^{1/2} > a \ln \left(\frac{\pi l}{4a} \right) \quad (4)$$

where a is a probe radius and l is a probe length (probe scale length is $\lambda_{pr} = a \ln(\pi l/(4a))$ [26]). The electron diffusion is given by $D_e = \nu \lambda/3$. The collision frequencies for electron–electron, electron–atom and electronic excitation are ν_e , ν_a and ν^* , respectively. Typical plasma parameters and probe dimensions are given in Table 1. The electronic excitation frequency is estimated by the electron–ion collision frequency for the present work. The term, $\delta = 2m/M$, is the electron–atom energy-transfer efficiency. In this instance, the kinetic equation for the distribution function can be simplified as a problem in spatial coordinates only [24]. The resulting solution for the electron current collected by the probe is given as follows:

$$I_e(U) = -\frac{8\pi e A_{pr}}{3m^2} \int_{eU}^{\infty} \frac{(W - eU)f(W)}{\gamma[1 + ((W - eU)/W)\psi(W)]} dW \quad (5)$$

where A_{pr} is the probe area, m and e are the electron mass and charge, respectively, U is the probe potential, W is the energy, γ is a geometric factor and $\psi(W)$ is the “diffusion parameter”. In the case of a magnetized plasma, the diffusion parameter is given as follows for a perpendicularly oriented probe [12,26]:

$$\psi_{\perp} = \frac{a \ln(\pi l/4a)}{\gamma R_{Le}(W, B)} \quad (6)$$

where $R_{Le}(W, B)$ is the electron Larmor radius. This equation is simplified such that a nominal value of the diffusion parameter is used at the Larmor radius corresponding to 1 eV such that $\psi(W) = \psi_0/\sqrt{W}$. An important consequence of having the full I - V characteristic available for interpretation is the ability to determine the plasma potential.

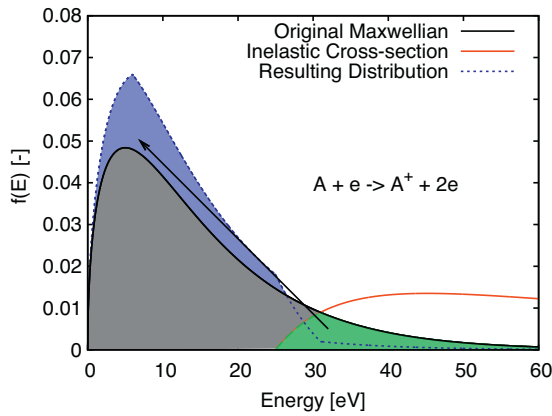


Fig. 1. Heuristic model of the effect of inelastic interactions (here ionization) on an initially Maxwellian distribution. The interacting particles are redistributed to lower energies as a result of the interaction.

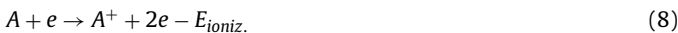
For large values of ψ_0 an approximation for Eq. (5) can be used such that the first derivative is found to be directly proportional to the distribution function [12,25]. This yields the result that:

$$f(\epsilon) \propto (eU)^{-3/2} \frac{dI}{dU} \quad (7)$$

This equation is a simplification of the full non-local interpretation where it was found that the error in using the approximation is less than 5% when the diffusion parameter is suitably large ($\psi_0 > 100$) [12]. The approximation is used in this study due to speed and simplicity of implementation with the expectation that the error in the derived distribution will be ≈ 10 –20%.

Ion-current growth far from floating potential is also considered here. It is modeled that the Debye sheath grows according to the Child-Langmuir law typical of flush-mount Langmuir probes [27]. In the thin-sheath regime, the effect of this ion-current growth is negligible for the classical interpretation, however, can impact the calculated distribution if not taken into account [26]. A typical sheath scale-length is of order micrometers while the projected probe size perpendicular to the incident magnetic field is 100s of micrometers confirming the thin-sheath regime.

A heuristic model demonstrating the impact of inelastic collisions (i.e. excitation and ionization) is described in texts [28] and the literature [18,29]. In such a case, an example reaction is considered as follows:



where A is some atom, e is the incident electron and E_{ioniz} is the energy lost to ionization. As a result of the interaction, the incident electron loses E_{ioniz} amount of energy. This process is depicted in Fig. 1 where a hypothetical cross-section is given with some threshold energy and interacts with an initially Maxwellian distribution. As reactions such as that shown in Eq. (8) occur, the reacted population above the ionization threshold is translated from higher to lower energies. This has the effect of creating a departure from a Maxwellian distribution. The degree to which the distribution departs from a Maxwellian is determined by the balance of the inelastic interactions and elastic (electron–electron) interactions [18].

In addition to atomic physics, non-local effects may alter the distribution function at any given location. The collision cross-section for charged-particles decreases with increasing energy [30] so that the mean-free-path decreases with increasing energy. In regions with steep gradients in plasma properties of density and temperature it is possible for these high-energy particles to originate in regions further away (hence the term “non-local”) than the slower

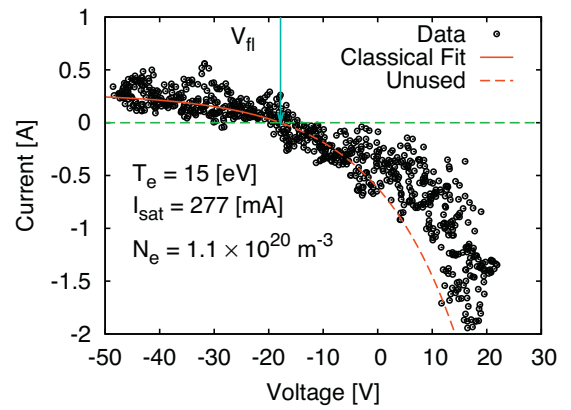


Fig. 2. Classical interpretation of Langmuir probe IV characteristic. Floating potential indicated by the arrow. Classical interpretation does not attempt to interpret data above floating potential, extension of the classical fit is shown for comparison.

particles. These non-local effects were the chief concern in the works by Chodura [16] and Batishchev et al. [17]. The degree of collisionality in the plasma is given by the ratio of a typical scale-length of the plasma with the mean-free-path of a given charged-particle population. In a tokamak, this can be defined with respect to the mid-plane plasma characteristics and total connection length of a given flux-tube [21]. As gradients in the near-surface plasma may be important, the following definition is used:

$$v_{ee}^* \equiv \frac{s}{\lambda_{ee}} \approx 10^{-16} \frac{n_e \cdot s}{T_e^2} \quad (9)$$

where v_{ee}^* is the electron–electron collisionality, s is the distance along the flux-tube from the PFC surface and λ_{ee} is the electron mean-free-path at a given energy. The collisionality is the ratio of the system scale-length with the mean-free-path of particle. In the work by Chodura [16], it was found that SOL collisionalities of about 10 would be insufficient to completely eliminate kinetic effects and that values of $v_{ee}^* \gtrsim 100$ with respect to the temperature scale-length are necessary. This is due to the fact that the parallel heat-flux is carried in electrons of energies $\approx 10T_e$.

3. Apparatus and approach

The liquid lithium divertor (LLD) has been installed in NSTX for the 2010 run campaign. It is described in detail in Refs. [5,31]. The Langmuir probe array used for this study is situated in between toroidal segments of the LLD and has been described elsewhere as well [7,8]. As mentioned above, the probes operate in the thin-sheath regime. In order to make contact with the non-local interpretation literature, the probes are approximated as a half-cylinder perpendicular to the magnetic field. This is possible as the inter-probe separation is a factor of ≈ 100 greater than the Debye sheath giving the probes the appearance of an isolated, proud structure rather than a flush-mounted one. In this way, the probe dimensions in this approximation yield $a \approx 6.1 \times 10^{-4}$ m and $l = 2 \times 10^{-3}$ m with corresponding diffusion parameter $\psi_0 \approx 40$. For all cases, the incident magnetic field angle is obtained from the magnetic reconstruction of the equilibrium with the EFIT code [32] interpolated between the nearest time points available ($\Delta t_{EFIT} = 9$ ms). The probes are swept at 500 Hz and sampled at 250 kSamples/s giving a sweep-to-sweep time of 1 ms. Three consecutive probe sweeps are overlaid for each analysis providing some mitigation of high-frequency random fluctuations.

The classical interpretation of the Langmuir probes is illustrated in Fig. 2. In this particular example, the fit is reasonable below the floating potential. Extending the fit beyond floating potential

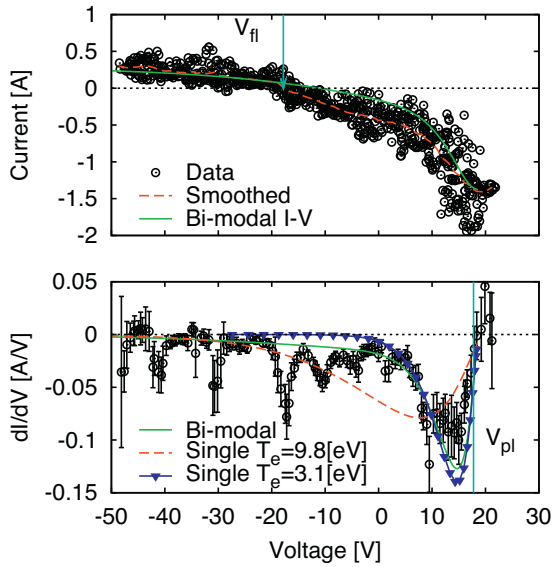


Fig. 3. I - V analysis steps for the determination of plasma potential. Identical data set as in Fig. 2 shown with adaptive smoothing result and calculated first derivative. Plasma potential is indicated at the zero crossing at ≈ 18 V. The model I - V characteristic of the bi-modal EEDF obtained by the analysis and Eq. (5) is shown in the upper figure. The model curves based on the obtained EEDF (Bi-modal) and two single-Maxwellian distributions ($T_e = 9.8$ and $T_e = 3.1$ eV) are also shown in the lower figure. See text for details.

however, illustrates the deviation from the expected exponential behavior.

The process of applying the non-local interpretation is as follows. First, the data are processed by a smoothing algorithm. This smoothing algorithm proceeds as a box-car averaging method, except that it applies a linear fit to the data (i.e. a moving regression). The slope of the linear fit and its uncertainty are used to estimate the derivative and its error at this point. The result of the smoothing algorithm and derivative calculation are shown in Fig. 3.

Fluctuations are identified in the data as follows: in the case of random noise, data is normally distributed about the mean. In the case of non-statistical fluctuations, as would arise from turbulent processes [33], say, the deviation from normal is manifest in the distribution of the data set. In a normal probability plot, this is demonstrated as a deviation from linearity and can be evaluated with the coefficient of determination [34]. When the mean coefficient of determination falls below a cutoff value for the entire data set, it is rejected from further processing on the grounds that it contains too large a variability. Additionally, this method allows the identification of features in the resulting analysis that may result from fluctuations arising from turbulence and aid in later interpretation.

Assuming the data set being analyzed is normally distributed about the smoothed curve, the next step is to determine the plasma potential. Model I - V characteristics are generated using a single Maxwellian distribution and Eq. (5). A χ^2 minimization routine is then utilized to determine which I - V characteristic and value of V_{plasma} best fit the data set. In the example shown in Fig. 3, the most prominent features are the zero-crossing location at 18 V and the minimum in dI/dV at about 12 V. Once the value of V_{plasma} is determined in this way the distribution function is calculated using Eq. (7). An example calculation is shown in Fig. 4.

Having obtained the distribution function and the model I - V characteristic, energy cutoffs are considered. The most important of these is the ion-current growth effect which, if not taken into account, would lead to a false high-energy tail [26]. The point at which sheath-growth effects come into play is calculated from the

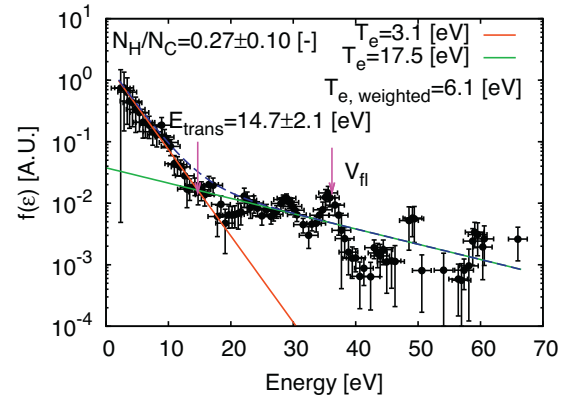


Fig. 4. Resulting electron distribution from the data shown in Figs. 2 and 3. In log-linear representation, a Maxwellian distribution is a straight line. The dashed line indicates the combination of both distributions. The obtained hot electron temperature is similar to that obtained by the classical analysis in Fig. 2.

model I - V characteristic and serves as a first cutoff for fitting. It has been found for the given diffusion parameter and typical plasma parameters at the divertor target that this cutoff is $\approx 9T_e$ for a single Maxwellian distribution. Below the cutoff energy, two models are applied to the data: a single Maxwellian distribution and a bi-modal distribution. The best-fit bi-modal distribution is determined by a χ^2 minimization algorithm that searches for the best transition in the data between distribution functions. The reduced χ^2 goodness-of-fit parameter is calculated for each which takes into account the number of degrees-of-freedom (DOFs) used in each. The goodness-of-fit serves as a method to distinguish whether the data are best described by either the single or bi-modal distributions.

Once the distribution is found in this manner, a new model curve is constructed with Eq. (5) and compared to the data set. This is shown in Fig. 3. Also shown in the figure are model curves constructed from two single-Maxwellian distributions. If one fits a single Maxwellian through the data shown in Fig. 4 the resulting temperature is $T_e = 9.8$ eV and this characteristic fails to reproduce the features above ≈ 0 V. If one creates an I - V characteristic from the bulk plasma temperature found in the bi-modal fitting algorithm, though only using a single-Maxwellian, then the derivative reaches zero far sooner than the data. Only the bi-modal I - V characteristic captures both features of the data, though none of the I - V characteristics can capture the fine-structure details such as that found between -20 and -10 V and this results in a slight discrepancy in the I - V characteristic.

The distribution functions obtained in this manner have the property that:

$$n = \int_0^{\infty} \sqrt{\epsilon} f(\epsilon) d\epsilon \quad (10)$$

With this, the ratio of densities, $\eta = n_h/n_c$ of the hot and cold electron populations can be calculated based on the fit parameters. The transition energy in the case of bi-modal distributions is also calculated. A density-weighted temperature is calculated for the bi-modal distributions as follows:

$$T_{e,bimodal} = \frac{T_{e,cold} + \eta T_{e,hot}}{1 + \eta} \quad (11)$$

The fraction of energy in the total plasma contained in the hot-electron fraction is given as $\eta T_{e,hot}$. Finally, with the determination of both floating and plasma potential, the estimate of $V_{plasma} - V_{fl} \approx 3T_e$ can be used to give another estimate of the temperature. The analysis code runs in an automated fashion and provides a consistent analysis method for finding V_{plasma} and the associated parameters of the distribution function. For the present

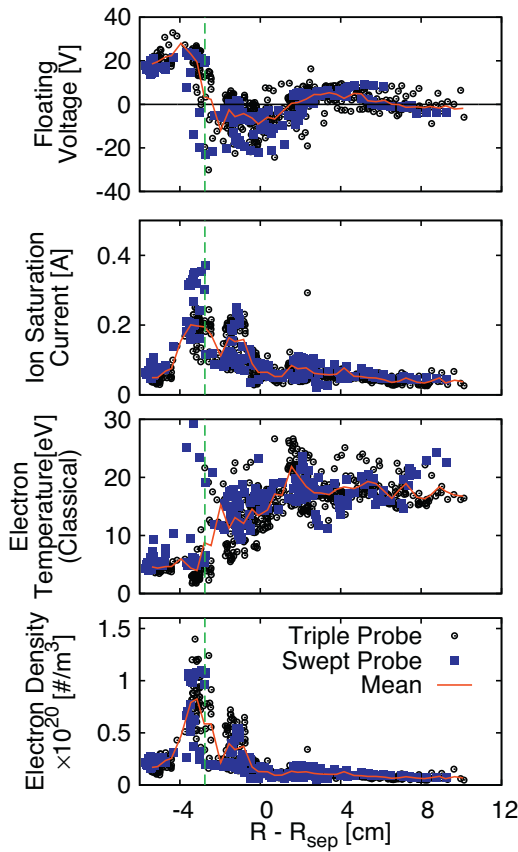


Fig. 5. Divertor plasma parameters obtained using classical interpretation and EFIT reference strike-point position. R_{sep} refers to EFIT strike-point position signal. Blue points are swept-probe results, black are 0.5 ms time averaged triple-probe measurements. Separatrix location determined by the peak in plasma pressure ($\approx n_e T_e$) is denoted by the vertical dashed line at -3 cm. The T_e profile is similar to that found in ASDEX [14] exhibiting a broad temperature “shoulder”. (For interpretation of the references to color in this figure legend, the reader is referred to the web version of this article.)

study, the data is reduced to the effective temperature and hot electron fractions to demonstrate the changes in the inferred EEDFs.

In order to provide a consistent inter-shot comparison, it is necessary to reference the Langmuir probes to some plasma location. This is done with the use of equilibrium reconstructions provided by EFIT [32]. For each time-point, the probe position is calculated as both a distance from the EFIT-determined strike-point and the value of the normalized magnetic flux on the surface. With this data processing, it is possible to construct the plasma profile as the strike-point sweeps back and forth over the Langmuir probes, as shown in Fig. 5. Similarly, it is possible to select a specific magnetic flux surface such that all probe measurements on that flux surface can be compared from shot to shot.

4. Results

Applying the non-local interpretation and equilibrium reconstruction techniques above, it is possible to make consistent analyses and comparisons on a shot-to-shot basis. The data are sorted for the magnetic surfaces corresponding ≈ 1 cm beyond the separatrix location (as determined by the peak in I_{sat}). Times considered are from 250 to 750 ms in the discharge.

During the course of experiments, a fueling scan was performed while plasma-bombardment heated the LLD plates (lithium evaporation was used and the rate maintained constant for all discharges). Based on known gas fueling rates, the number of electrons

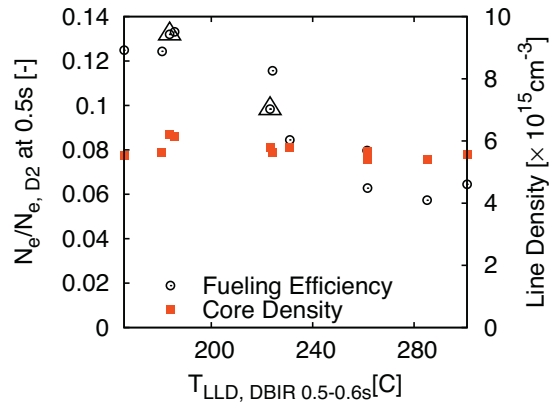


Fig. 6. Fueling efficiency and line-integrated electron density vs. mean plate temperature from 500 to 600 ms for the experimental sequence considered. Discharges utilized for detailed comparison are indicated by the large open triangles.

due to D_2 fueling can be calculated and compared to the plasma electron content calculated by volume integration of the density from multi-point Thomson scattering measurements. The ratio of electrons in the plasma divided by the nominal electrons supplied by the gas fueling rates is interpreted as a fueling efficiency. Fig. 6 shows the results of this fueling scan. During the course of LLD plate heating, the line-integrated core density of electrons did not significantly change whereas the fueling efficiency decreased by a factor of two. It should be noted that more than one ion species is present in the NSTX plasma and these exhibit some complex behavior, though the total electron content remained constant. The interested reader is referred to the associated paper on the LLD performance [31]. The loss of fueling efficiency implies an increase in absorption. In order to assess if local plasma conditions were changing during this sequence, two discharges were considered for detailed analysis; these are indicated in Fig. 6. The discharges were chosen as the plasma shaping is most similar and the ELMing character is also the same (Type-V ELMs reappeared toward the end of this discharge sequence whereas they are absent in the shots considered). These two discharges are referred to by the mean LLD plate-surface temperature for the time period of 500–600 ms as measured by the dual-band IR system: 184C and 224C.

Fig. 7 shows the results of the non-local interpretation comparing the plasma and floating potentials for the SOL region. Most striking is the variation in floating potential which is the simplest and most direct measurement that can be made with a Langmuir

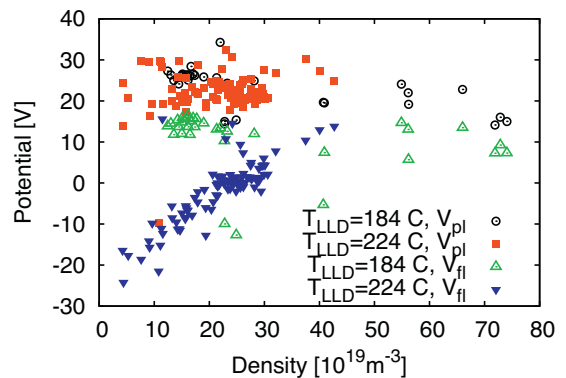


Fig. 7. Measured V_{float} and inferred V_{plasma} as a function of density during the two discharges considered on identical ψ surfaces in the SOL. Measurements indicate that the reduction in floating potential cannot be explained by a similar reduction in plasma potential.

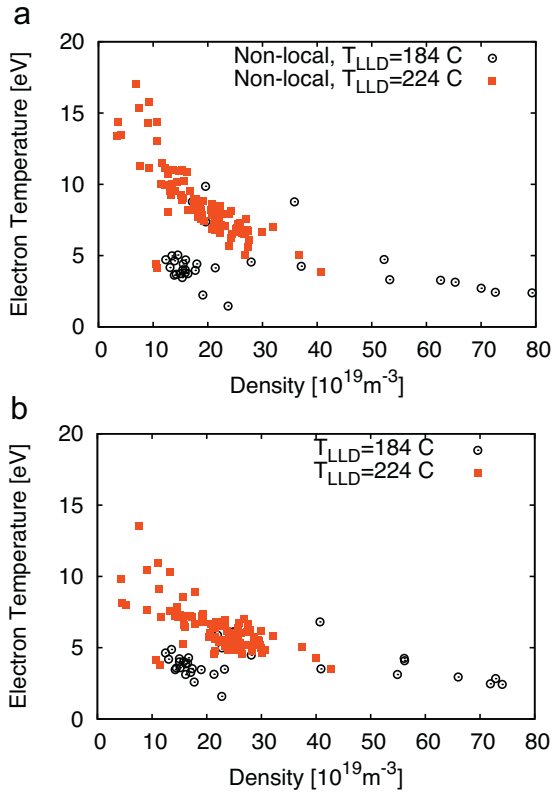


Fig. 8. (a) Temperatures and densities inferred by the difference between plasma and floating potentials ($T_e \propto V_p - V_f$) and (b) calculated from the analyzed bimodal distribution. Both analyses indicate a rise in temperature for the discharge with the higher mean plate temperature (density-weighted T_e).

probe. In the latter discharge, it is found that the floating potential is depressed from $\approx +10$ V to the range of ≈ -25 to $+5$ V in the latter discharge. The non-local analysis indicates that the plasma potential does not change a significant amount between the two discharges and cannot provide a simple accounting for the change in floating potential.

Fig. 8(a) and (b) shows comparisons of the electron temperatures for the two discharges considered. The electron temperature is calculated in two ways: from the difference between plasma and floating potentials and from the fitted distribution functions. The two discharges show a separation in temperature for both calculation methods. This is more pronounced with the potential-difference method but both calculation methods indicate a higher electron temperature is present in the latter discharge where the LLD surface was hotter. For comparison, Fig. 9 shows the electron temperature calculated with the classical method and the two non-local methods. The classical method results in consistently higher temperatures by almost a factor of two whereas the similarity between the two non-local T_e calculation methods indicates the internal consistency in the method.

The change in potential difference is most strongly correlated with the energy contained in the inferred hot-electron fraction. This is shown in Fig. 10. Comparisons were also made to the density ratio, η , and the cold electron energy fraction. Table 2 summarizes the differences between the three correlations tested.

5. Discussion and conclusions

Interpretive fluid modeling was carried out with the OEDGE (OSM + EIRENE + DIVIMP edge) code suite [35] in order to assess the degree of collisionality in the NSTX SOL. The OEDGE modeling

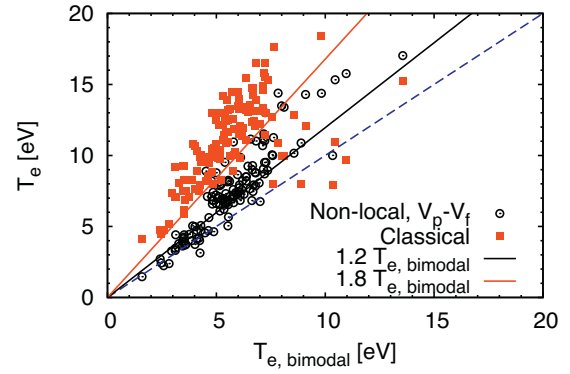


Fig. 9. Comparison of electron temperature measurements obtained from three methods of calculation. The density-weighted bimodal temperature is shown on the abscissa and is compared to T_e calculated from $V_p - V_f$ and as calculated from the classical interpretation [8]. Best-fit trends are shown for comparison. The potential-difference method yields temperatures 20% higher than the bimodal temperature on average whereas the classical method is 80% higher on average.

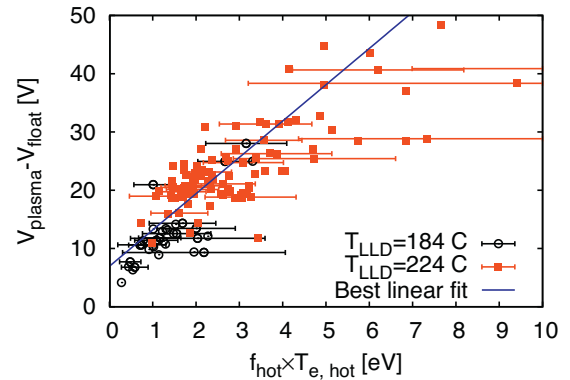


Fig. 10. Difference between plasma and floating potential as a function of the energy contained in the hot electron fraction. Representative error bars shown on subset of data for clarity.

code operates by taking density and temperature derived from Langmuir probes or other measurements as an input and then integrates the 1D fluid equations along a flux tube (Onion-Skin Model or OSM) to generate a plasma solution. Once a background plasma is solved in this way, the EIRENE [36] neutral transport code is used to simulate the recycling deuterium and the solution is used again as source terms for the OSM solution. The final solution is obtained after iterating between OSM and EIRENE a number of times. For this simulation a high-recycling wall composed of graphite was used with the plasma properties obtained from the classical interpretation method. The plasma solution is shown in Fig. 11 as a function of parallel distance from the target. The particular magnetic surface selected is slightly outboard of the separatrix location. It can be seen that steep gradients exist in the plasma solutions of density and temperature immediately adjacent to the target, and a significant amount of ionization is found adjacent to the target as well. The electron collisionality is shown for the nominal electron temperature and also for two multiples of this temperature. This

Table 2

Summary of correlation analyses on $V_p - V_f$. Linear function is fit to the data and the reduced χ^2 goodness-of-fit metric is used to evaluate.

Variable	Reduced χ^2 metric
Hot elec., $\eta T_{e,hot}$	0.75
Density ratio, η	1.47
Cold elec., $(1 - \eta) T_{e,cold}$	11.73

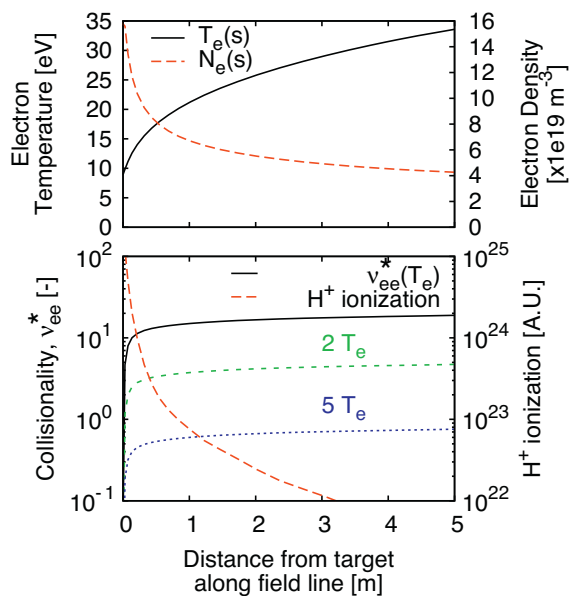


Fig. 11. Plasma fluid solution obtained with OEDGE code. At top, plasma density and temperature are shown as a function of distance along a field line from the target. At bottom, the collisionality parameter corresponding to the obtained fluid solution and two multiples of the background temperature solution. Hydrogen ionization rate also shown in the lower figure.

comparison gives some indication of the variance of collisionality for electrons of higher energy than the thermal population. The collisionality is not found to be high enough to rule out kinetic effects [16] and the sharp gradients in the SOL as well as large amount of electron–neutral interactions adjacent to the PFC also indicate that non-Maxwellian distributions are probable. More detailed OEDGE modeling and comparison of the two interpretation methods as well as the resulting plasma solutions is planned for future work.

The non-local interpretation method and associated magnetic flux surface selection rules yield consistent (in terms of sweep-to-sweep analysis) results on the shots compared. This is most clearly seen in Fig. 7 in the obtained plasma potential. In comparing the classical with the non-local methods, it is found that the classical method yields temperatures almost twice as high as the density-weighted bi-modal temperatures as shown in Fig. 9. This is expected in plasmas with an energetic tail fraction and this effect has been shown in the literature [12]. Additionally, it was predicted by Batishchev that such distribution functions in the divertor would lead to over-estimates of the electron temperature by a factor of 2–6 [17]. Further indication that the inferred kinetic effects are occurring is found by examination of infrared thermography. It has been found by Kallman et al. [37] that the classical probe interpretation yields a calculated sheath heat transmission coefficient in NSTX of 2–3, significantly lower than the expected value of ≈ 7 . This could be due to a bi-modal distribution altering the probe measurements [13]. A more detailed study of these effects is planned.

The non-local interpretation yields electron temperatures that are higher in the latter discharge studied where the LLD surface temperature was higher. The first indication of this difference in near-surface plasma conditions is in the variation of floating potential and the classical interpretation method also provides an indication that the latter discharge had higher temperatures. In the classical interpretation, though, it is impossible to evaluate plasma potential, so the non-local approach is necessary to assess whether the change in floating potential was significant. With the non-local approach it is found that the increase in potential difference between V_{plasma} and V_{float} is most strongly correlated with the energy contained in the hot-electron fraction, indicated in Fig. 10.

A number of items can contribute to a change in the hot electron fraction. The heuristic model describing the impact of electron–neutral interactions shows that a reduction in the number of these interactions would increase the population of hot electrons reaching the PFC. The ion saturation current is, in fact, higher in the latter discharge and so this implies that the PFC would be absorbing more incident plasma in the latter discharge. A variation in the gradients in the SOL adjacent to the PFC could also contribute to a change in the measured distribution. In this case, an increase in the hot-electron fraction implies the PFC is absorbing more incident plasma [16]. Both effects are the subject of ongoing studies.

The increase in local electron temperature, reduced fueling efficiency, and increase in the hot-electron fraction are all consistent with an absorbing PFC.

Initial tests with the LLD have been performed in NSTX. Local plasma modifications have been measured with the Langmuir probes applying both the classical and the non-local interpretation methods. Overall machine performance indicates a decrease in fueling efficiency and the Langmuir probes show an increase in near-surface plasma temperature. The increase in plasma-to-floating potential difference is most strongly correlated with an increase in the hot-electron energy fraction. Preliminary fluid modeling indicates that kinetic effects are likely to exist in the NSTX SOL. The increase in hot-electron fraction, increase in temperature, reduction in machine-fueling efficiency are all consistent with an absorbing PFC developing as the LLD surface temperature increased.

Acknowledgements

The authors would like to thank Y. Raitses for many useful discussions regarding the Langmuir probe interpretation and E. Spence for discussions on data analysis and reduction methods. This work is supported under Department of Energy contract No. DE-AC02-09CH11466.

References

- [1] J.D. Strachan, D.K. Mansfield, M.G. Bell, J. Collins, D. Ernst, K. Hill, et al., Wall conditioning experiments on TFTR using impurity pellet injection, *Journal of Nuclear Materials* 217 (1994) 145–153.
- [2] R. Majeski, R. Doerner, T. Gray, R. Kaita, R. Maingi, D. Mansfield, et al., Enhanced energy confinement and performance in a low-recycling tokamak, *Physical Review Letters* 97 (2006) 075002.
- [3] G. Mazzitelli, M.L. Apicella, V. Pericoli-Ridolfini, G. Apruzzese, R. De Angelis, A. Romano, et al., Review of FTU results with the liquid lithium limiter, *Fusion Engineering and Design* 85 (2010) 896–901.
- [4] M.G. Bell, H.W. Kugel, L.E. Zakharov, H. Schneider, B.P. LeBlanc, D. Mansfield, et al., Plasma response to lithium-coated plasma-facing components in the national spherical torus experiment, *Plasma Physics and Controlled Fusion* 51 (2009) 124054.
- [5] H.W. Kugel, M.G. Bell, L. Berzak, A. Brooks, R. Ellis, S. Gerhardt, et al., Physics design requirements for the national spherical torus experiment liquid lithium divertor, *Fusion Engineering and Design* 84 (2009) 1125–1129.
- [6] H.W. Kugel, M.G. Bell, H. Schneider, J.P. Allain, R.E. Bell, R. Kaita, et al., Lithium coatings on NSTX plasma facing components and its effects on boundary control, core plasma performance and operation, *Fusion Engineering and Design* 85 (2010) 865–873.
- [7] J. Kallman, M.A. Jaworski, R. Kaita, H.W. Kugel, T.K. Gray, High density Langmuir probe array for NSTX SOL measurements under lithiated divertor conditions, *Review of Scientific Instruments* 81 (2010) 10E117.
- [8] M.A. Jaworski, J. Kallman, R. Kaita, H.W. Kugel, B.P. LeBlanc, R. Marsala, et al., Biasing, acquisition, and interpretation of a dense Langmuir probe array in NSTX, *Review of Scientific Instruments* 81 (2010) 10E130.
- [9] G. Matthews, Tokamak plasma diagnosis by electrical probes, *Plasma Physics and Controlled Fusion* 36 (1994) 1595–1628.
- [10] P. Stangeby, Effect of bias on trapping probes and bolometers for tokamak edge diagnosis, *Journal of Physics D: Applied Physics* 15 (1984) 1007–1029.
- [11] J. Tagle, P. Stangeby, S. Erents, Errors in measuring electron temperatures using a single Langmuir probe in a magnetic field, *Plasma Physics and Controlled Fusion* 29 (1987) 297–301.
- [12] T. Popov, P. Ivanova, J. Stockel, R. Dejarnac, Electron energy distribution function, plasma potential and electron density measured by Langmuir probe in tokamak edge plasma, *Plasma Physics and Controlled Fusion* 51 (2009) 065014.

- [13] P. Stangeby, A problem in the interpretation of tokamak Langmuir probes when a fast electron component is present, *Plasma Physics and Controlled Fusion* 37 (1995) 1031–1037.
- [14] G. Fussman, U. Ditte, W. Eckstein, T. Grave, M. Keihacker, K. McCormick, et al., Divertor parameters and divertor operation in ASDEX, *Journal of Nuclear Materials* 128–129 (1984) 350–358.
- [15] J.G. Watkins, P. Stangeby, J.A. Boedo, T.N. Carlstrom, C.J. Lasnier, R.A. Moyer, et al., Comparison of Langmuir probe and Thomson scattering measurements in DIII-D, *Journal of Nuclear Materials* 290–293 (2001) 778–782.
- [16] R. Chodura, Kinetic effects in the scrape off layer, *Contributions to Plasma Physics* 32 (1992) 219–230.
- [17] O.V. Batishchev, S.I. Krasheninnikov, P.J. Catto, A.A. Batishchev, D.J. Sigmar, X.Q. Xu, et al., Kinetic effects in tokamak scrape-off layers plasmas, *Physics of Plasmas* 4 (1997) 1672–1680.
- [18] D. Tskhakaya, S. Jachmich, T. Eich, W. Fundamenski and JET EFDA Contributors, Interpretation of divertor Langmuir probe measurements during ELMs at JET, *Journal of Nuclear Materials*, 415 (2011) S860–S864.
- [19] J. Swift, M. Schwar, *Electrical Probes for Plasma Diagnostics*, American Elsevier Publishing Company, Inc., New York, 1994.
- [20] M. Liebermann, A. Lichtenberg, *Principles of Plasma Discharges and Materials Processing*, John Wiley & Sons, Inc., New York, 1994.
- [21] P.C. Stangeby, *The Plasma Boundary of Magnetic Fusion Devices*, Institute of Physics Publishing, Philadelphia, 2000.
- [22] V. Pericoli Ridolfini, R. Zagorski, F. Crisanti, G. Granucci, G. Mazzitelli, L. Pieroni, et al., Characterisation of the scrape-off layer plasma in the FTU tokamak, *Journal of Nuclear Materials* 220–222 (1995) 218–222.
- [23] Y.B. Golubovskii, V.M. Zakharova, V.N. Pasunkin, L.D. Tsendin, Probe measurements of the electron energy distribution under diffusion conditions, *Soviet Journal of Plasma Physics* 7 (1981) 340–344.
- [24] R. Arslanbekov, N. Khromov, A. Kudryavtsev, Probe measurements of electron energy distribution function at intermediate and high pressures and in a magnetic field, *Plasma Sources, Science and Technology* 3 (1994) 528–538.
- [25] V.I. Demidov, S.V. Ratynskaia, R.J. Armstrong, K. Rypdal, Probe measurements of electron energy distributions in a strongly magnetized low-pressure helium plasma, *Physics of Plasmas* 6 (1999) 350–358.
- [26] V.A. Godyak, V.I. Demidov, Probe measurements of electron-energy distributions in plasmas: what can we measure and how can we achieve reliable results? *Journal of Physics D: Applied Physics* 44 (2011) 269501.
- [27] J.P. Gunn, C. Boucher, D. Desroches, A. Robert, Operation of flush-mounted probes in the TdeV tokamak, *Review of Scientific Instruments* 68 (1997) 404–407.
- [28] V.E. Golant, A.P. Zhilinsky, I.E. Sakharov, S.C. Brown, *Fundamentals of Plasma Physics*, John Wiley & Sons, New York, 1980.
- [29] V. Demidov, S. Ratynskaia, K. Rypdal, Electric probes for plasmas: the link between theory and instrument, *Review of Scientific Instruments* 73 (2002) 3409–3439.
- [30] T. Boyd, J. Sanderson, *The Physics of Plasmas*, Cambridge University Press, Cambridge, UK, 2003.
- [31] H.W. Kugel, J.P. Allain, M.G. Bell, R.E. Bell, R. Ellis, S.P. Gerhardt, et al., NSTX plasma operation with a liquid lithium divertor, *Fusion Engineering and Design* (2011), these proceedings.
- [32] S.A. Sabbagh, S.M. Kaye, J. Menard, F. Paoletti, M.G. Bell, R.E. Bell, et al., Equilibrium properties of spherical torus plasmas in NSTX, *Nuclear Fusion* 41 (2001) 1601–1611.
- [33] P. Davidson, *Turbulence, An introduction for scientists and engineers*, Oxford University Press, Oxford, UK, 2004.
- [34] P. Bevington, D. Robinson, *Data reduction and error analysis for the physical sciences*, second ed., McGraw-Hill, Inc., New York, 1992.
- [35] P.C. Stangeby, J.D. Elder, J.A. Boedo, B. Bray, N.H. Brooks, M.E. Fenstermacher, et al., Interpretative modeling of simple-as-possible-plasma discharges on DIII-D using the OEDGE code, *Journal of Nuclear Materials* 313–316 (2003) 883–887.
- [36] D. Reiter, Progress in two-dimensional plasma edge modelling, *Journal of Nuclear Materials* 196–198 (1992) 80–89.
- [37] J. Kallman, M.A. Jaworski, R. Kaita, H.W. Kugel, A.G. McLean and V. Surla, Effective sheath heat transmission coefficient in NSTX discharges with applied lithium coatings (2011), these proceedings.